

# The FreeEOS Code for Calculating the Equation of State for Stellar Interiors III: The Treatment of the Coulomb Correction

Alan W. Irwin

*Department of Physics and Astronomy, University of Victoria,  
P.O. Box 3055, Victoria, British Columbia, Canada, V8W 3P6  
Electronic mail: [irwin@beluga.phys.uvic.ca](mailto:irwin@beluga.phys.uvic.ca)*

## ABSTRACT

This paper describes how the Coulomb correction is implemented in FreeEOS (<http://freeeos.sourceforge.net/>), a software package for rapidly calculating the equation of state for physical conditions in stellar interiors.

*Subject headings:* Coulomb interaction — equation of state — stellar interiors — stellar evolution

## 1. Introduction

FreeEOS (<http://freeeos.sourceforge.net/>) is a software package for rapidly calculating the equation of state (hereafter, EOS) for stellar conditions, and a series of papers is being prepared that describe its implementation. Paper I (Irwin 2004a) describes the Fermi-Dirac integral approximations. Paper II (Irwin 2004b) describes the efficient method of solution that delivers thermodynamically consistent results of high numerical quality that are in excellent agreement with OPAL (Rogers & Nayfonov 2002) results for the solar case. Here in this third paper in the series, I present the implementation of the Coulomb correction. This non-ideal correction accounts for the tendency of oppositely charged, unbound particles to correlate with each other because of the attractive Coulomb forces between them. Because of this net attraction between the correlated particles, less pressure is generally required to confine the gas to a particular volume for a given temperature. An accurate treatment of the Coulomb correction is essential since this correction is one of the most important non-ideal corrections to the EOS calculation for stellar-interior conditions.

The remainder of this paper is organized as follows: Section 2 presents our recommended model for the Coulomb free energy as well as various other models I have programmed as a basis for comparison, while Sections 3, 4, and 5 give results, discussion, and conclusion.

## 2. The Coulomb Free Energy

The general expression adopted for the Coulomb free energy employs the following definitions for the Coulomb sums  $\Sigma_0^C$  and  $\Sigma_2^C$ , the weak Coulomb interaction parameter  $\Lambda$ , and the strong Coulomb interaction parameter  $\Gamma$ :

$$\Sigma_0^C \equiv \sum_{\Pi} n_{\Pi}, \quad (1)$$

$$\Sigma_2^C \equiv \sum_{\Pi} n_{\Pi} Z_{\Pi}^2, \quad (2)$$

$$\Lambda \equiv \frac{2e^3 \pi^{1/2} (\Sigma_2^C + n_e \theta_e)^{3/2}}{(4\pi \epsilon_0 kT)^{3/2} (\Sigma_0^C + n_e \theta_e)}, \quad (3)$$

and

$$\Gamma \equiv (\Lambda/3^{1/2})^{2/3} = \frac{e^2}{4\pi \epsilon_0 kT} \frac{(4\pi/3)^{1/3} \Sigma_2^C + n_e \theta_e}{(\Sigma_0^C + n_e \theta_e)^{2/3}}. \quad (4)$$

The number density of the positive ion identified by index  $\Pi$  is given by  $n_{\Pi}$ , the charge on that positive ion is given by  $Z_{\Pi}$ , and

$$\theta_e \equiv \partial \ln n_e(\eta, T) / \partial \eta, \quad (5)$$

where  $n_e$  is the number density of free electrons and  $\eta$  is a degeneracy parameter. I describe the approximation used for  $n_e(\eta, T)$  in Paper I, and  $\theta_e$  is calculated from the analytical derivative of that approximation. (Note all units in this paper are SI unless specified otherwise. Furthermore, throughout this paper the symbol  $\ln$  will stand for the natural logarithm and the symbol  $\log$  will stand for the base 10 logarithm.) Using the above definitions, the adopted expression for the Coulomb free energy reduces to

$$F_C = -kTV(\Sigma_0^C + n_e \theta_e) g_C(\Gamma), \quad (6)$$

where  $g_C(\Gamma)$  is the so-called Coulomb function.

These expressions for  $\Lambda$ ,  $\Gamma$ , and  $F_C$  are the same as those used by Pols et al. (1995, PTEH), except we have replaced  $\Sigma_0^C$  in their formulation by  $\Sigma_0^C + n_e \theta_e$ . In the limit of small degeneracy (which correlates with small  $\Gamma$ ),  $\theta_e$  approaches unity, and our formulation reduces to the DeWitt (1969) formulation. In the limit of large degeneracy (which correlates with large  $\Gamma$ ),  $\theta_e$  approaches zero and our formulation reduces to the PTEH formulation. The recommended Coulomb function,  $g_C(\Gamma)$ , is discussed in the following sub-sections.

### 2.1. Constraints on the recommended Coulomb function and associated free energy

For small  $\Gamma$  the recommended Coulomb function should approach the Debye-Hückel (DH) result,

$$g_{\text{DH}}(\Gamma) \equiv \Gamma^{3/2} / 3^{1/2}. \quad (7)$$

This small- $\Gamma$  constraint on the Coulomb function insures the corresponding recommended Coulomb free-energy will approach

$$F_{\text{DH}} = -kTV(\Sigma_0^{\text{C}} + n_e\theta_e)\Lambda/3, \quad (8)$$

which for small degeneracy gives the same result that can be derived from first principles using an activity expansion of the grand canonical partition function (Rogers 1994).

For large  $\Gamma$  the recommended Coulomb function should approach the one-component-plasma (OCP) result which is well represented by

$$g_{\text{OCP}}(\Gamma) = a\Gamma + b\Gamma^s + c \ln \Gamma + d, \quad (9)$$

where  $a = 0.899126$ ,  $b = -0.60712/s$ ,  $s = 0.321308$ ,  $c = 0.27998$ , and  $d = 0.436484 - a - b$  (see DeWitt, Slattery, & Chabrier 1996, DSC). This large- $\Gamma$  constraint on the Coulomb function insures the corresponding Coulomb free-energy approximates liquid, multi-component-plasma (LMCP) results which are well represented by the linear mixing rule,

$$F_{\text{LMCP}} = -kTV \sum_{\Pi} n_{\Pi} g_{\text{OCP}}(Z_{\Pi}^{5/3} \Gamma_0), \quad (10)$$

where

$$\Gamma_0 = \frac{e^2}{4\pi\epsilon_0 kT} \left( \frac{4\pi}{3} \Sigma_1^{\text{C}} \right)^{1/3} \quad (11)$$

and

$$\Sigma_1^{\text{C}} \equiv \sum_{\Pi} n_{\Pi} Z_{\Pi}. \quad (12)$$

For large degeneracy,  $\theta_e \approx 0$ ; and for large  $\Gamma$ ,  $g_{\text{OCP}} \approx a\Gamma$ . Under these conditions, the relative difference between the Coulomb free energy corresponding to  $g_{\text{OCP}}$  and the LMCP result is

$$\frac{\Sigma_0^{\text{C}} \Gamma}{\sum_{\Pi} n_{\Pi} Z_{\Pi}^{5/3} \Gamma_0} - 1 = \frac{(\Sigma_0^{\text{C}})^{1/3} \Sigma_2^{\text{C}}}{(\Sigma_1^{\text{C}})^{1/3} \Sigma_{5/3}^{\text{C}}} - 1, \quad (13)$$

where

$$\Sigma_{5/3}^{\text{C}} \equiv \sum_{\Pi} n_{\Pi} Z_{\Pi}^{5/3}. \quad (14)$$

Note both equation (9) and equation (10) are not exact representations of the definitive DSC Monte Carlo results, but I have ignored these representation errors in this development since, in general, they are small compared to the relative error given by equation (13).

## 2.2. The Recommended Coulomb Function

In the FreeEOS implementation the recommended Coulomb function is represented by

$$\log g_{\text{C}} \equiv Y(X), \quad (15)$$

where  $X \equiv \log \Gamma$  and  $Y(X)$  is characterized by the two fitting parameters  $X_{\text{DH}}$  and  $X_{\text{OCP}}$ . For all  $X$  values less than or equal to  $X_{\text{DH}}$ ,  $Y$  is set equal to the DH result,  $\log g_{\text{DH}}$ , which more than satisfies the small- $\Gamma$  constraint on  $g_{\text{C}}$  discussed in Section 2.1. For all  $X$  values greater than or equal to  $X_{\text{OCP}} > X_{\text{DH}}$ ,  $Y$  is set equal to the modified OCP result,  $\log(g_{\text{OCP}} + \delta c \ln \Gamma + \delta d)$ , which satisfies the large- $\Gamma$  constraint on  $g_{\text{C}}$  discussed in Section 2.1.  $X_{\text{DH}} = -0.4$  and  $X_{\text{OCP}} = 0$ . give the best fit of FreeEOS results to OPAL results (see Sect. 3) and these values are adopted for the recommended Coulomb function.

The parameters  $\delta c$  and  $\delta d$  are internally adjusted in the FreeEOS implementation to give a cubic polynomial in the transition region between  $X_{\text{DH}}$  and  $X_{\text{OCP}}$  that is continuous in  $Y(X)$ ,  $Y'(X)$ , and  $Y''(X)$  with DH results at  $X = X_{\text{DH}}$  and with modified OCP results at  $X = X_{\text{OCP}}$ . The basic equations that must be satisfied by that cubic are given in Sect.3.3 of Press et al. (1986). The cubic is determined by the 4 requirements of  $Y(X)$  and  $Y''(X)$  continuity at  $X = X_{\text{DH}}$  and  $X = X_{\text{OCP}}$ . However, for the unmodified OCP result (i.e.,  $\delta c = 0$  and  $\delta d = 0$ ), the first derivatives are non-continuous. To make them continuous, a Newton-Raphson iteration procedure is used to solve the two  $Y'(X)$  continuity constraints in terms of the two unknowns  $\delta c$  and  $\delta d$ . This procedure is only done once for a particular set of  $X_{\text{DH}}$  and  $X_{\text{OCP}}$  values, and the resulting  $\delta c$  and  $\delta d$  values tend to be small so that modified OCP results from the recommended Coulomb function do not strongly differ from unmodified OCP results for large  $\Gamma$  values (see Sect. 3).

### 2.3. Other Models for the Coulomb Free Energy

The recommended treatment of the Coulomb free energy (i.e., eq. [6] with the Coulomb function,  $g_{\text{C}}(\Gamma)$ , constructed as in Sect. 2.2) has been designed to join the Debye-Hückel approximation smoothly with a good approximation to LMCP results using the Coulomb fitting parameters  $X_{\text{DH}} = -0.4$  and  $X_{\text{OCP}} = 0$ . This treatment is part of the EOS1 free-energy model option suite (described in Paper I) that gives a good fit to OPAL solar results (see Paper II). However, I have implemented additional Coulomb free-energy model options for FreeEOS. These options provide variations on the EOS1 option suite that reduce the required computer time to perform the EOS calculations. Also these options (in combination with other FreeEOS options) provide almost exact emulation of the PTEH; Swenson, Irwin, & Rogers, (unpublished, SIREFF); or Mihalas, Däppen, & Hummer (1988, MDH) equations of state.

#### 2.3.1. Approximations for the Coulomb Sums

The form of the Coulomb free energy (eq. [6]) implies the associated correction to the equilibrium constants given by equation (35) of Paper II depends on the auxiliary variables  $\Sigma_0^{\text{C}}$  and  $\Sigma_2^{\text{C}}$  defined by equations (1) and (2). Normally, these auxiliary variables are determined to high numerical precision as part of the EOS solution by Newton-Raphson iteration as discussed in Pa-

per II, but the FreeEOS implementation also offers two options for approximating these auxiliary variables. These approximations save computer time by reducing the number of auxiliary variables that need to be determined by iteration.

The ‘‘PTEH’’ approximations for the Coulomb sums are taken from the PTEH reference, and are given as follows:

$$\Sigma_0^C \approx n_e \Sigma_0^+ / \Sigma_1^+ \quad (16)$$

and

$$\Sigma_2^C \approx n_e \Sigma_2^+ / \Sigma_1^+; \quad (17)$$

where for  $k = 0, 1, 2$

$$\Sigma_k^+ = \sum_j \epsilon_j Z_j^k. \quad (18)$$

The  $j$  index runs over all elements,  $Z_j$  is the nuclear charge (atomic number), and

$$\epsilon_j = X_j / A_j. \quad (19)$$

$X_j$  is the abundance by weight,  $A_j$  is the atomic weight, and  $\sum_j X_j \equiv 1$ . The approximations given by equations (16) and (17) are exact if all elements are un-ionized or completely ionized. Furthermore, these approximations require evaluation of no auxiliary variables.

The ‘‘SIREFF’’ approximations for the Coulomb sums are taken from the SIREFF EOS implementation and are given as follows:

$$\Sigma_0^C \approx n(H^+) + n(He^+) + n(He^{++}) + \frac{n(H^+)}{\epsilon(H)} \sum_m \epsilon_m \quad (20)$$

and

$$\Sigma_2^C \approx n(H^+) + n(He^+) + 4n(He^{++}) + \frac{n(H^+)}{\epsilon(H)} \sum_m \epsilon_m + \frac{n(He^{++})}{\epsilon(He)} \sum_m \epsilon_m (Z_m^2 - 1); \quad (21)$$

where the  $m$  index runs over just the metals. Equations (20) and (21) are exact in the limits where all elements are un-ionized, singly ionized or completely ionized. These approximations normally require knowledge of no additional auxiliary variables when using the SIREFF free-energy model. For that model,  $n(H_2^+)$  is ignored (which is why that species is not included in the above equations), and  $n(H^+)$ ,  $n(He^+)$ , and  $n(He^{++})$  are already required auxiliary variables for the SIREFF form of pressure ionization.

### 2.3.2. Additional Options for the Coulomb Treatment

Other Coulomb options available for FreeEOS users are as follows.

- (1) Ignore the Coulomb effect.

- (2) Replace  $X_{\text{DH}} = -0.4$  and  $X_{\text{OCP}} = 0.$  by  $X_{\text{DH}} = -1.$  and  $X_{\text{OCP}} = 0.$
- (3) Replace  $\Sigma_0^{\text{C}} + n_e \theta_e$  wherever it appear in the recommended formulation by  $\Sigma_0^{\text{C}}.$
- (4) Replace the recommended Coulomb function by the PTEH version (see their eq. [25]),

$$g_{\text{PTEH}}(\Gamma) = \frac{a_1 \Gamma}{\{[\Gamma/(\Gamma + a_3)]^{1/a_2} + (a_1 \sqrt{3/\Gamma})^{1/a_2}\}^{a_2}}, \quad (22)$$

where  $a_1 = 0.89752,$   $a_2 = 0.768,$  and  $a_3 = 0.208.$

- (5) Replace the recommended  $\theta_e$  (see discussion following eq. [5]) by the PTEH version (which is based on their eq. [29]).
- (6) Replace the recommended Coulomb function by the Debye-Hückel version  $g_{\text{DH}}$  (eq. [7]).
- (7) Replace the recommended Coulomb function by a corrected Debye-Hückel version  $\tau(x)g_{\text{DH}};$  where

$$\tau(x) = 3x^{-3}[\ln(1+x) - x + x^2/2] \quad (23)$$

(eq. [11] from MDH),

$$x \equiv \left[ \frac{2\pi^{1/2} e^3 n_e}{(4\pi\epsilon_0 kT)^{3/2}} \right] \frac{F_{1/2}(\eta, 0)}{F_{3/2}(\eta, 0)} \frac{(\Sigma_2^{\text{C}} + \theta_e n_e)^{1/2}}{\Sigma_0^{\text{C}}}, \quad (24)$$

and  $F_k(\eta, 0)$  is the non-relativistic limit of the Fermi-Dirac integral of order  $k$  (see Paper I).

Options (1) and (2) above are useful for studies (e.g., Cassisi, Salaris, & Irwin 2003) of the sensitivity of stellar-interior results to the overall Coulomb effect and variations in the approximation for the Coulomb effect at intermediate  $\Gamma$ ; the combination of the PTEH approximations for the Coulomb sums and options (3) through (5) above constitute the PTEH Coulomb model; the combination of the SIREFF approximations for the Coulomb sums and option (6) above constitute the SIREFF Coulomb model; and precise iterative calculation of the Coulomb sums and option (7) above constitute the MDH Coulomb model.

### 3. Results

Figure 1 gives the recommended  $\log g_{\text{C}};$  its first two derivatives; and residuals of  $\log g_{\text{DH}},$   $\log g_{\text{OCP}},$  and  $\log g_{\text{PTEH}}$  relative to  $\log g_{\text{C}}.$  By design, the recommended  $g_{\text{C}}$  and its first and second derivative are continuous and agree with  $g_{\text{DH}}$  for  $\log \Gamma \leq X_{\text{DH}} = -0.4.$  Because of the continuity constraint discussed in Sect. 2.2,  $\delta c$  and  $\delta d$  are non-zero so that  $\log g_{\text{C}}$  differs from  $\log g_{\text{OCP}}$  by 0.095 at  $X = 0.,$  but these differences decrease with increasing  $X.$  The differences between  $g_{\text{C}}$  and  $g_{\text{PTEH}}$  are discussed in the next section.

To give the following results and discussion some context, Figure 2 compares EOS quantities and the loci of several stellar interior models on the density-temperature plane for solar metallicity. The high-density, low-temperature calculation limit indicated in the figure is defined by

$$\log \rho_{\text{lim}} = \log \rho_5 + (3/2) \log(T/10^5) \quad (25)$$

for  $\log T < 6$  and continued by the  $\log T = 6$  isotherm. The limit parameter of  $\log \rho_5 = 3.3$  is used for this figure to avoid regions where FreeEOS calculations currently do not converge. This calculation limit roughly corresponds to a  $0.1-M_{\odot}$  model and can also be viewed as the approximate limit of validity for FreeEOS calculations (see further discussion in Paper II). This same  $\log \rho_5$  limit parameter is also used for all other  $\rho, T$  figures in this paper except for Figure 4.

Figure 3 shows the overall change in pressure due to the Coulomb effect. In general, the Coulomb effect increases with increasing density and decreasing temperature, but this overall trend is modified by other factors which affect the EOS. The Coulomb effect is reduced at high densities because the pressure from degenerate electrons grows faster than the Coulomb pressure, at high temperatures because the ideal pressure increases with temperature while the Coulomb pressure decreases, combined high temperatures and low densities because the radiation pressure dominates the pressure, at low densities because the mean distance between particles is low (and therefore interactions are reduced), and at low temperatures because of low ionization (fewer charged particles to interact). The net result of all these different effects is as illustrated; for fixed abundance the Coulomb effect is largest at combined intermediate densities and intermediate temperatures corresponding to the envelopes of extreme lower-main-sequence stars. In general, for fixed abundance and any given stellar model the Coulomb effect first increases inward as ionization is increased, reaches a maximum in the envelope, and then decreases inward as the temperature is increased still further. Note in contrast to the fixed abundance case, the Coulomb effect may increase inward near the core of models in advanced stages of stellar evolution because the effect goes as the cube of the charge on the ions (see eqs. [3] and [8]) which monotonically increases as a function of time due to nuclear processing.

Figure 4 shows the pressure effect of changing the model for the Coulomb function from the recommended  $g_C$  to  $g_{\text{DH}}$ . The two FreeEOS calculations being compared are identical by definition for  $\log \Gamma \leq X_{\text{DH}} = -0.4$  (see Fig. 1), but as the  $\Gamma$  value is increased the two calculations rapidly diverge to the point where the FreeEOS calculation that uses  $g_{\text{DH}}$  produces unphysical results (e.g., negative overall pressures) for physical conditions that are typical for envelopes of extreme LMS stars. This illustrates why a non-DH Coulomb approach is required for such conditions.

Figures 5 through 7 show the effect of changing the model for the Coulomb function from the recommended  $g_C$  to  $g_{\text{PTEH}}$ . Figure 5 shows the overall change in pressure, while figures 6 and 7 show more detailed results for the locus of points in a solar-mass model and a  $0.1-M_{\odot}$  model. The model results will be discussed in detail in the next section.

#### 4. Discussion

The Coulomb functions  $g_C$  and  $g_{\text{PTEH}}$  are continuous in at least the function and its first and second derivatives. This is a necessary condition for second-order thermodynamic quantities like  $\Gamma_1$  (which depend on a second-order partial derivative of the free-energy) to be continuous. Furthermore,  $g_C$  and  $g_{\text{PTEH}}$  satisfy the small- and large- $\Gamma$  constraints presented in Section 2.1. Thus, the EOS results corresponding to these Coulomb functions make a smooth transition from DH results at small  $\Gamma$  to an approximation to LMCP results at large  $\Gamma$ . However, Figure 1 shows that  $g_{\text{PTEH}}$  has significant differences with  $g_C$ . For  $\log \Gamma \leq X_{\text{DH}} = -0.4$ , these differences are identical to the differences of  $g_{\text{PTEH}}$  relative to  $g_{\text{DH}}$  while for  $\log \Gamma \geq X_{\text{OCP}} = 0.$ , these differences are essentially the negative of the differences between  $g_C$  and  $g_{\text{OCP}}$ .

Figure 6 presents FreeEOS results as a function of the model depth variable  $T(r)$  in a solar-mass model. The first panel of the figure shows how  $\Gamma_1$  behaves with depth to indicate important EOS transitions such as the combined hydrogen and first helium ionization zone (the primary minimum in  $\Gamma_1$ ) and the the second helium ionization zone (the secondary minimum in  $\Gamma_1$ ). The remaining panels of the figure show how the differences between  $g_{\text{PTEH}}$  and  $g_C$  (and essentially the differences between  $g_{\text{PTEH}}$  and  $g_{\text{DH}}$  since the maximum solar  $\log \Gamma$  value is only slightly larger than  $X_{\text{DH}} = -0.4$ ) propagate to various thermodynamic quantities for the locus of points in a solar-mass model.

To help predict the effect of the illustrated residuals on derived solar properties it is important to remember that in the adiabatic part of the solar convection zone,  $P$  becomes an implicit function of  $\rho$  along an adiabat. Once the adiabatic exponent,  $\Gamma_1 = \partial \ln P(\rho, s) / \partial \ln \rho$  is known along the adiabat (defined by constant entropy per unit mass,  $s$ ), the solution for the density-depth and pressure-depth relations,  $\rho(r)$  and  $P(r)$  follows from the boundary conditions on the adiabatic region and solution of Poisson’s equation (see discussion in Cox and Giuli 1968, Sect. 19.1). The temperature-depth relation,  $T(r)$  is then determined from the EOS relation  $T(\rho(r), P(r))$  in the adiabatic region. The residuals in  $\Gamma_1$  tend to be oscillatory as illustrated in the figure because  $\Gamma_1$  is a second-order thermodynamic quantity. These oscillatory residuals should have little effect on  $\rho(r)$  and  $P(r)$  outside the adiabatic region. In contrast, the EOS relation  $P(\rho(r), T(r))$  is a first-order thermodynamic quantity (it depends on a first partial derivative of the free energy) so  $\ln P(\rho(r), T(r))$  residuals tend to be systematic as illustrated in the figure. The residuals in the  $\ln T(\rho(r), P(r))$  relation should similarly be systematic (although opposite in sign). So long as these systematic residuals as illustrated in this figure do not propagate to the surface or to the deep part of the model where the luminosity is generated, and so long as the residuals in  $\ln \rho(r)$  and  $P(r)$  do not propagate outside the adiabatic zone, then the radius and luminosity of the model should largely be unaffected by EOS changes or uncertainties in the adiabatic part of the model.

In contrast to the case of the predicted radius and luminosity of the sun, the predicted acoustic periods of the sun should be significantly affected (at least compared to the high level of accuracy with which the solar acoustic periods have been observationally determined) by the difference

between  $g_{\text{PTEH}}$  and  $g_{\text{DH}}$ . The predicted acoustic periods are largely determined by the integral of the inverse sound speed over depth, and the change in adopted Coulomb function affects the sound speed at the  $10^{-2}$  level right where the integrand is fairly near its maximum value. Furthermore, comparison of this plot with Figures 6 and 7 of Paper II, shows use of  $g_{\text{PTEH}}$  completely destroys the good agreement we have with the OPAL EOS for the solar case. In fact, in all the attempts to adjust the EOS1 option suite to fit the OPAL results, I have never been able to improve on simply adopting the Debye-Hückel Coulomb function,  $g_{\text{DH}}$ , for the solar case. It is for this reason that I have designated  $g_{\text{C}}$  (which is essentially identical to  $g_{\text{DH}}$  in the solar case by design) as the recommended Coulomb function and use that function rather than  $g_{\text{PTEH}}$  in the EOS1 option suite.

Figure 7 shows the same quantities as Figure 6 except that all calculations have been done for a  $0.1-M_{\odot}$  model. The envelope conditions of this model are near the limit of validity of the current EOS1 option suite of FreeEOS because of deficiencies in the adopted pressure ionization scheme. In fact, the current pressure-ionization model for the metals is much less detailed than it is for hydrogen and helium, and this oversimplification causes near-discontinuous metal ionization and the accompanying sharp changes that occur for  $\Gamma_1$  and other quantities (for example, near  $\log T(r) = 5.7$ ).

The Coulomb effect is large ( $\log \Gamma > 0$ ) through much of the  $0.1-M_{\odot}$  model with the maximum  $\log \Gamma$  value approaching 0.5 in the envelope. Thus, through much of the model  $g_{\text{PTEH}}$  will give a better approximation to  $g_{\text{OCP}}$  than  $g_{\text{C}}$ , and a FreeEOS calculation with  $g_{\text{PTEH}}$  will give a better approximation to LMCP results than the  $g_{\text{C}}$  calculation. Nevertheless, except for the outermost layers the model is completely convective, and because of the high densities involved almost all but the outermost layers are adiabatic as well. Under these conditions (as discussed for the solar-mass model), the largely oscillatory nature of the  $\Gamma_1$  residuals and lack of systematic  $\ln P(\rho(r), T(r))$  residuals at the surface and at depth indicate that the predicted radius and luminosity of the  $0.1-M_{\odot}$  model should largely be unaffected by using  $g_{\text{C}}$  rather than  $g_{\text{PTEH}}$ . An even stronger argument can be made for the relative error of the current Coulomb formulation compared to the linear-mixing rule formulation for large  $\Gamma$ . Indeed, for normal helium abundances the maximum  $n(\text{He}^{++})/n(\text{H}^+)$  value is approximately 0.10, and the maximum error estimated from equation 13 is only 3 % which is an order of magnitude smaller than the relative differences between  $g_{\text{PTEH}}$  and  $g_{\text{C}}$  shown in Figure 1.

## 5. Conclusions

This paper has described how the Coulomb correction is implemented in the FreeEOS software library. The recommended set of Coulomb options that are used in the EOS1 option suite smoothly join Debye-Hückel results at weak Coulomb coupling to a good approximation to liquid, multi-component-plasma results for strong Coulomb coupling. The match with the Debye-Hückel results is maintained to a sufficiently large value of the Coulomb coupling constant ( $\log \Gamma = -0.4$ ) to secure an excellent fit to OPAL results for the solar case (see Figs. 6 and 7 of Paper II). This Coulomb

treatment should be suitable for most stellar-interior calculations with the notable exception of the cool white dwarfs where the phase transition to a crystalline state is encountered for large Coulomb coupling.

The FreeEOS software library is licensed under the GPL and is freely downloadable from <http://freeeos.sourceforge.net/>. Older versions of FreeEOS used a spline fit to approximate the Coulomb implementation introduced at version 1.4.0 of FreeEOS and described in this paper.

I thank Forrest Rogers for many useful discussions; Santi Cassisi for providing some representative model calculations and for his friendly encouragement of my FreeEOS work; Ben Dorman, Fritz Swenson, and Don Vandenberg for helping to arouse my original interest in the EOS problem for stellar interiors; and Richard Stallman, Linus Torvalds, and many other programmers for the GNU/Linux computer operating system and accompanying tools that have made it practical to develop the FreeEOS code on personal computers. The figures of this paper have been generated with the yPlot (<http://yplot.sourceforge.net>) and PLplot (<http://www.plplot.org>) scientific plotting packages.

## REFERENCES

- Cassisi, S., Salaris, M., & Irwin, A.W. 2003, *ApJ*, 588, 862
- Cassisi, S. 2005, private communication
- Cox, J. P., & Giuli, R. T. 1968, *Principles of Stellar Structure* (New York: Gordon and Breach)
- DeWitt, H. E. 1969, in *Low Luminosity Stars*, ed. S. Kumar (New York: Gordon and Breach), p. 211
- DeWitt, H., Slattery, W., & Chabrier, G. 1996, *Physica B228*, 21 (DSC)
- Irwin, A.W. 2004a, [http://freeeos.sourceforge.net/eff\\_fit.pdf](http://freeeos.sourceforge.net/eff_fit.pdf) (Paper I)
- Irwin, A.W. 2004b, <http://freeeos.sourceforge.net/solution.pdf> (Paper II)
- Mihalas, D., Däppen, W., & Hummer, W. G. 1988, *ApJ*, 331, 815 (MDH)
- Pietrinferni, A., Cassisi, S., Salaris, M., & Castelli, F. 2004, *ApJ*, 612, 168
- Pols, O. R., Tout, C. A., Eggleton, P. P., & Han, Z. 1995, *MNRAS*, 274, 964 (PTEH)
- Press, W.H., Flannery, B.P., Teukolsky, S.A., & Vetterling, W. T. 1986, *Numerical Recipes* (Cambridge, Cambridge University Press)
- Rogers, F. J. 1994, in *The Equation of State in Astrophysics IAU Coll. 147*, ed. G. Chabrier, E. Schatzman (Cambridge: Cambridge University Press), p. 16
- Rogers, F.J. & Nayfonov, A. 2002, *ApJ*, 576, 1064 (OPAL)

Fig. 1.— The recommended  $Y(X) = \log g_C$  and its first two derivatives as a function of  $X = \log \Gamma$  and comparison of  $\log g_{\text{DH}}$ ,  $\log g_{\text{OCP}}$ , and  $\log g_{\text{PTEH}}$  with  $Y$  as a function of  $X$ .  $Y(X)$  smoothly joins DH results with modified OCP results using a cubic polynomial (see text).

Fig. 2.— A solar-metallicity comparison of EOS quantities and loci of model stellar interiors. The thin short-dashed line indicates where the radiative and gas pressures are equal and is the boundary between the radiation-dominated and matter-dominated EOS. The thin solid lines indicate the middle of important ionization and dissociation zones. The “He<sup>+</sup>”, “He”, “H”, and “H<sub>2</sub>” labels respectively correspond to where half the helium is singly ionized or neutral and where half the hydrogen is in neutral monatomic form or in the diatomic molecular form. The medium thickness solid line indicates the current high-density, low-temperature calculation limit for FreeEOS (see text). The thick solid lines indicate  $\rho, T$  loci of model stellar interiors provided by Cassisi (2005). These models were calculated using the EOS1 option suite of FreeEOS and the stellar-evolution code that has been described in Pietrinferni, et al. (2004). The labels of “0.1”, “0.3”, “1.0”, “RGT”, and “CG” respectively indicate main-sequence models of 0.1, 0.3, and 1.0  $M_\odot$  and models of 1.0  $M_\odot$  evolved to the tip of the red-giant branch and to the initial clump-giant phase (zero-age horizontal branch of solar metallicity).

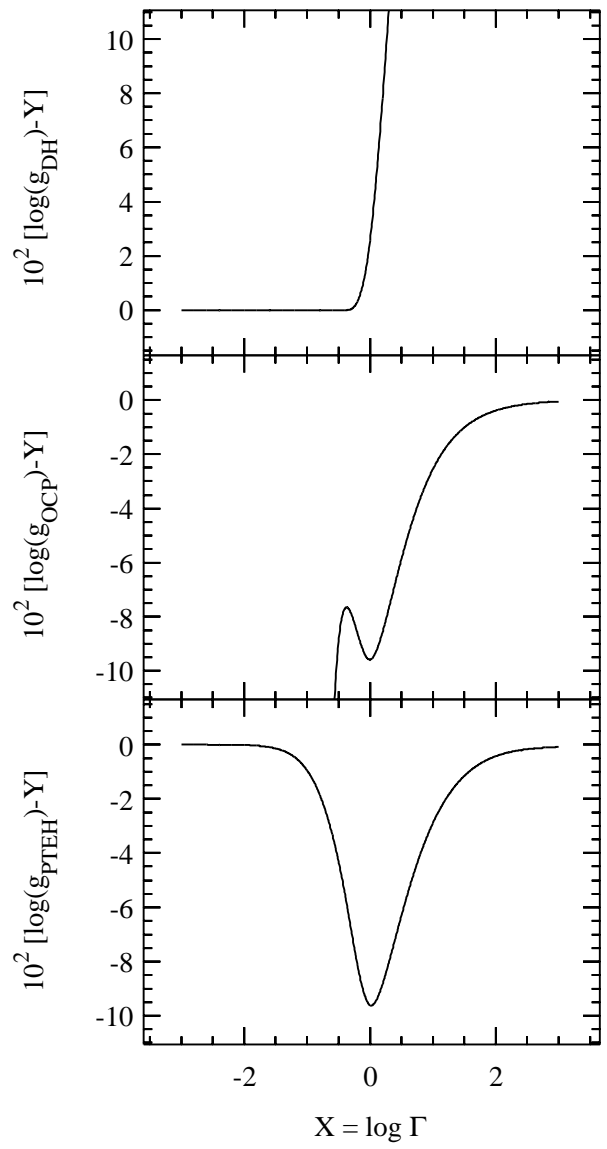
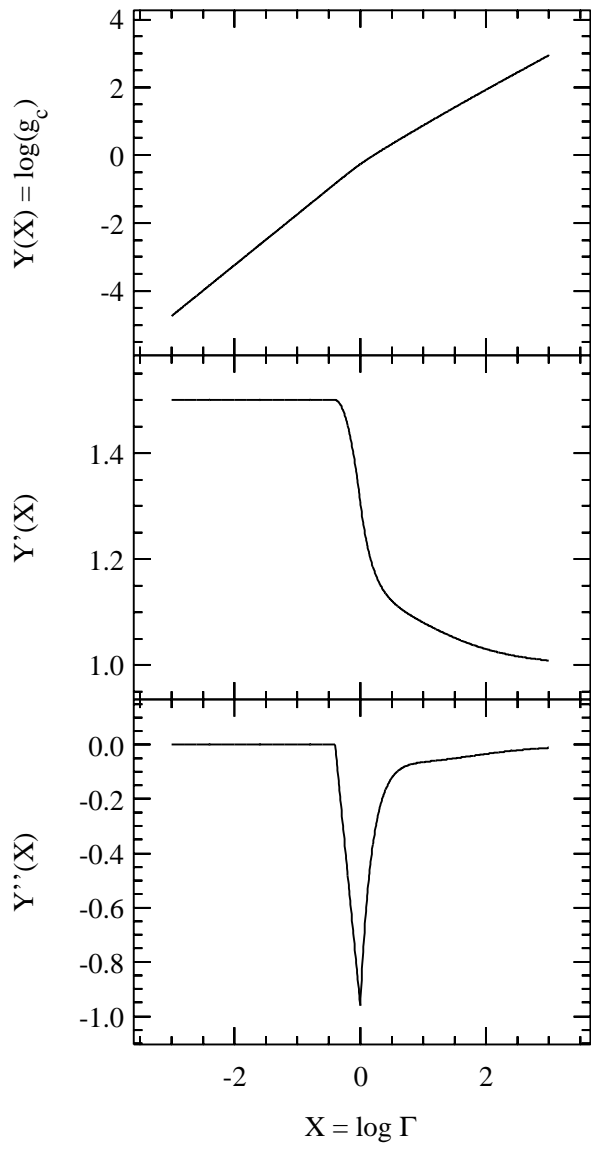
Fig. 3.— The log of the relative change in pressure caused by changing from the recommended free-energy model to one where the Coulomb free-energy component is dropped. Solar abundances were used for both EOS calculations employed in the comparison. The high-density, low-temperature calculation limit is the same as in Figure 2.

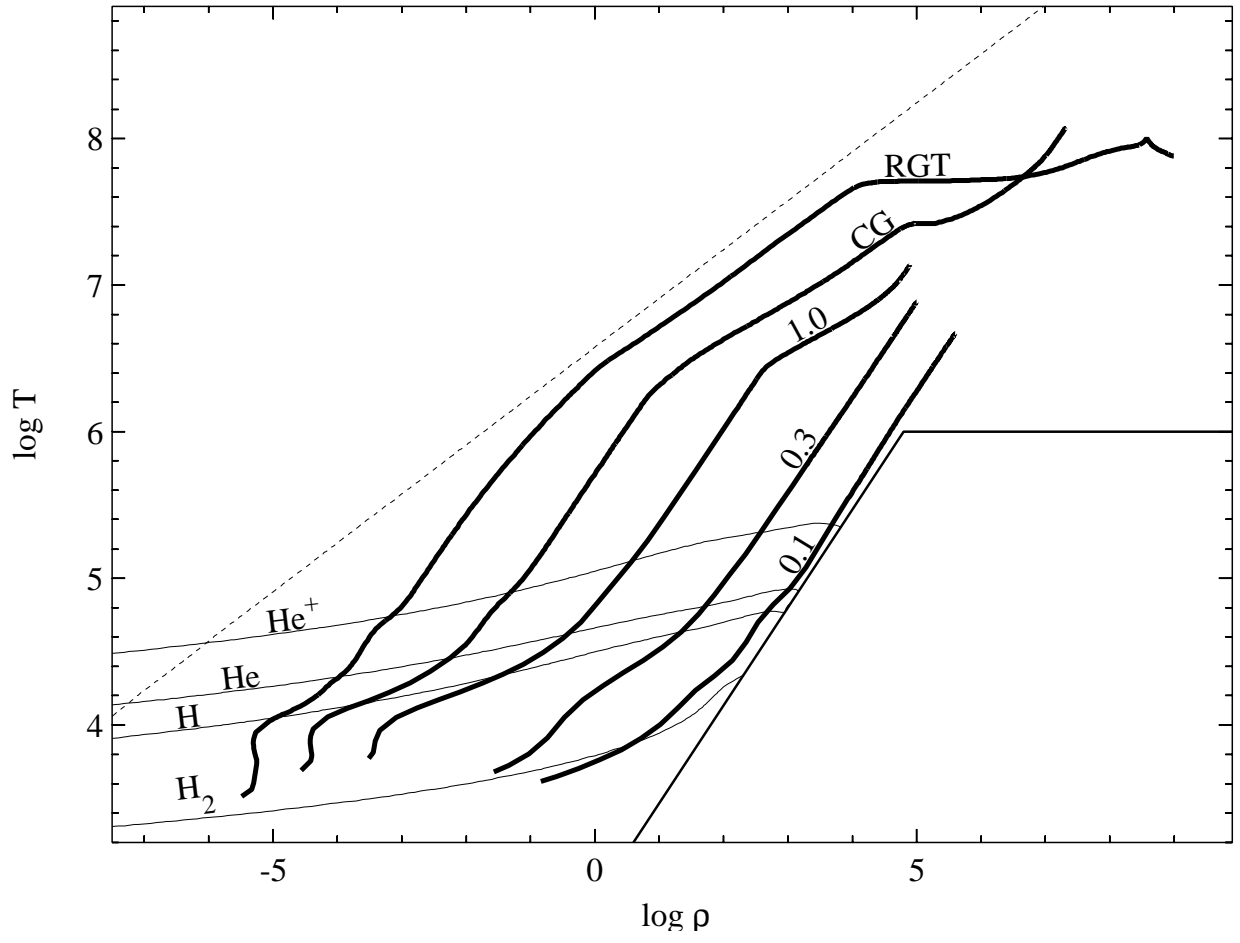
Fig. 4.— The log of the relative change in pressure caused by changing from the recommended Coulomb free-energy model to one where  $g_C$  is replaced by  $g_{\text{DH}}$  (eq. [7]). Solar abundances were used for both EOS calculations employed in the comparison. To avoid negative pressures for the DH case, the high-density, low-temperature calculation limit was shifted to lower densities by 1.05 dex (i.e.,  $\log \rho_5$  was reduced from 3.3 to 2.25).

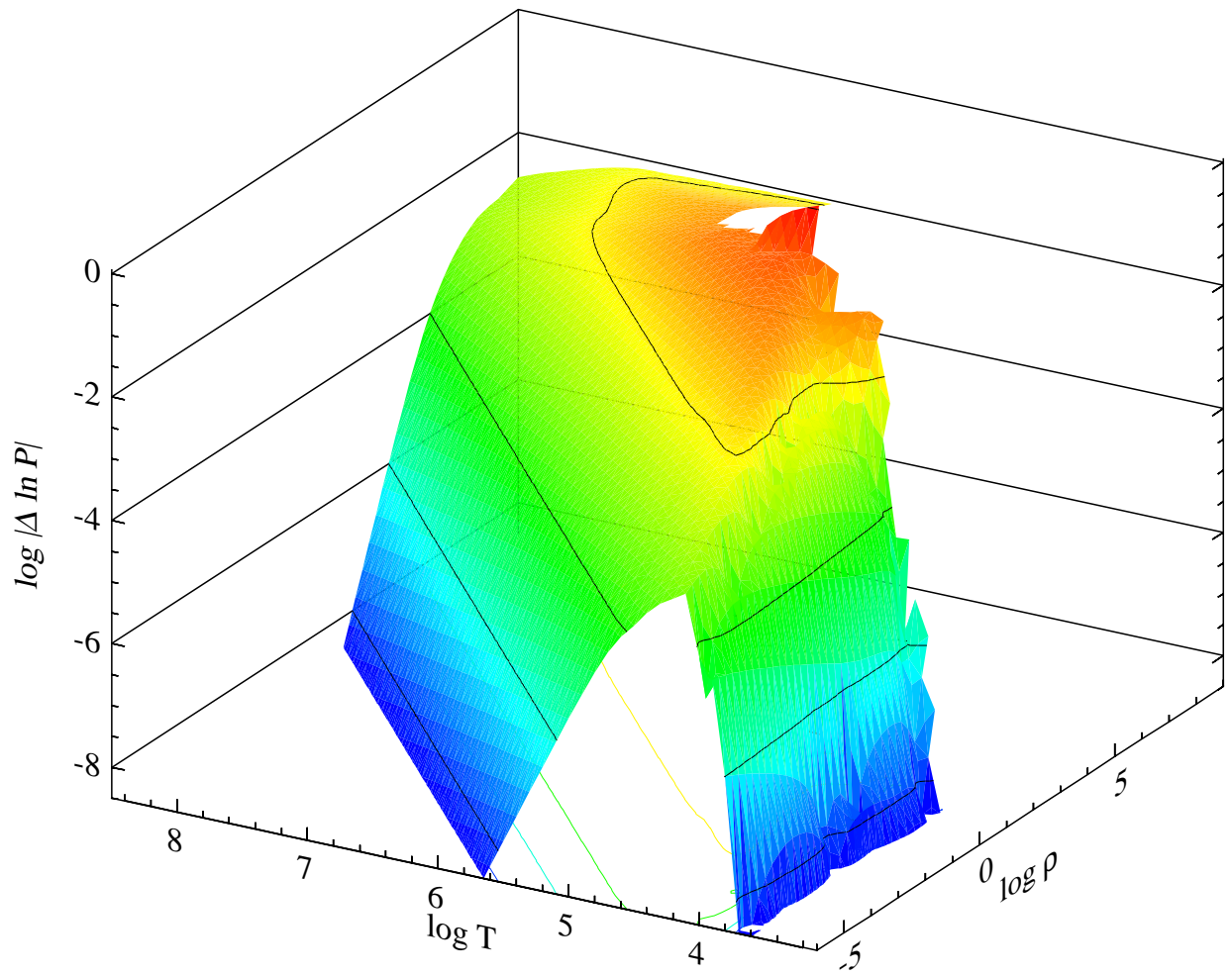
Fig. 5.— The log of the relative change in pressure caused by changing from the recommended Coulomb free energy model to one where  $g_C$  is replaced by  $g_{\text{PTEH}}$  (eq. [22]). Solar abundances were used for both EOS calculations employed in the comparison. The high-density, low-temperature calculation limit is the same as in Figure 2.

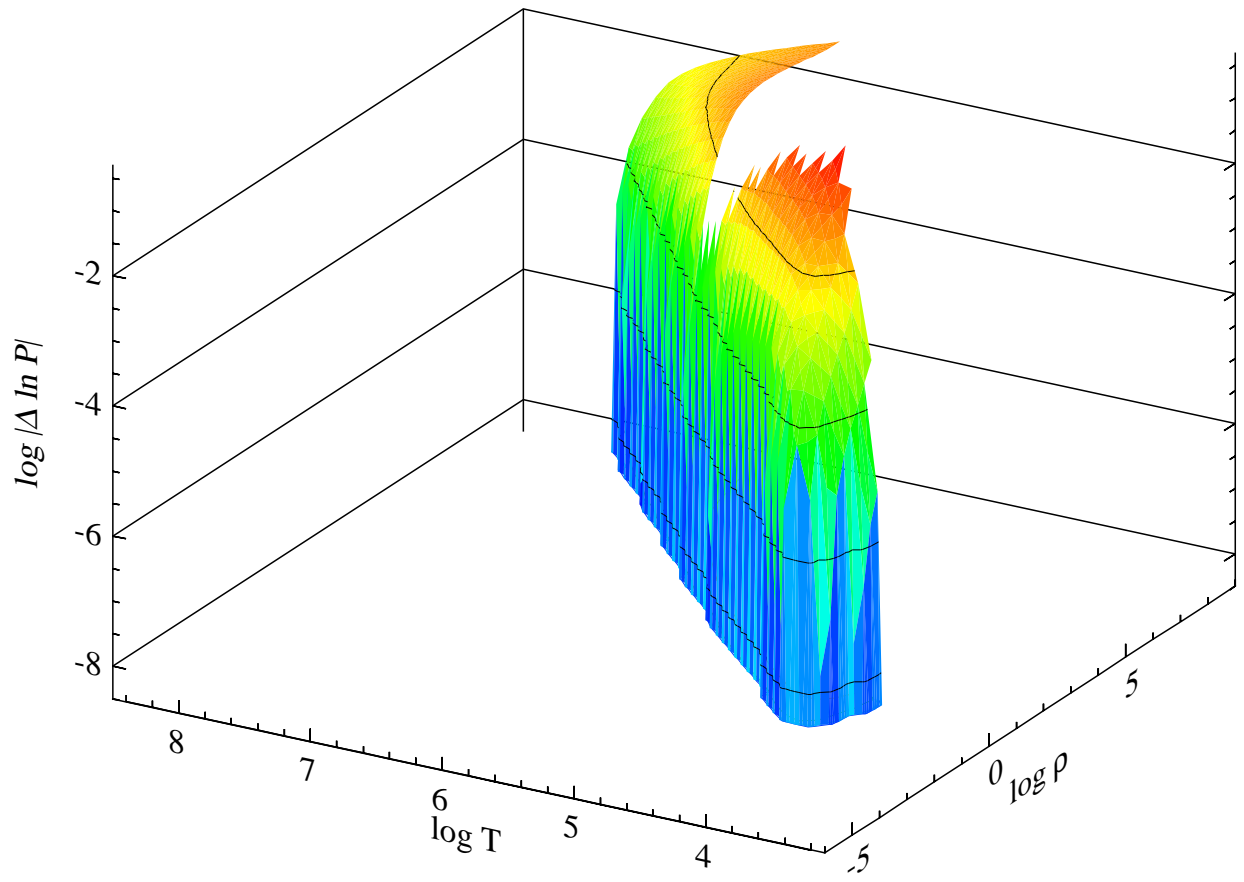
Fig. 6.— The adiabatic pressure gradient,  $\Gamma_1$ , for the recommended Coulomb free-energy model as well as the the change in  $\Gamma_1$ , relative change in  $P$ , and the log of the relative change in the square of the sound speed,  $v_s^2 = \Gamma_1 P / \rho$ , as a function of the temperature of each depth point for a solar-mass model. The plotted changes are derived from two independent FreeEOS calculations; one with the recommended Coulomb treatment and one where  $g_C$  has been replaced by  $g_{\text{PTEH}}$  (eq. [22]).

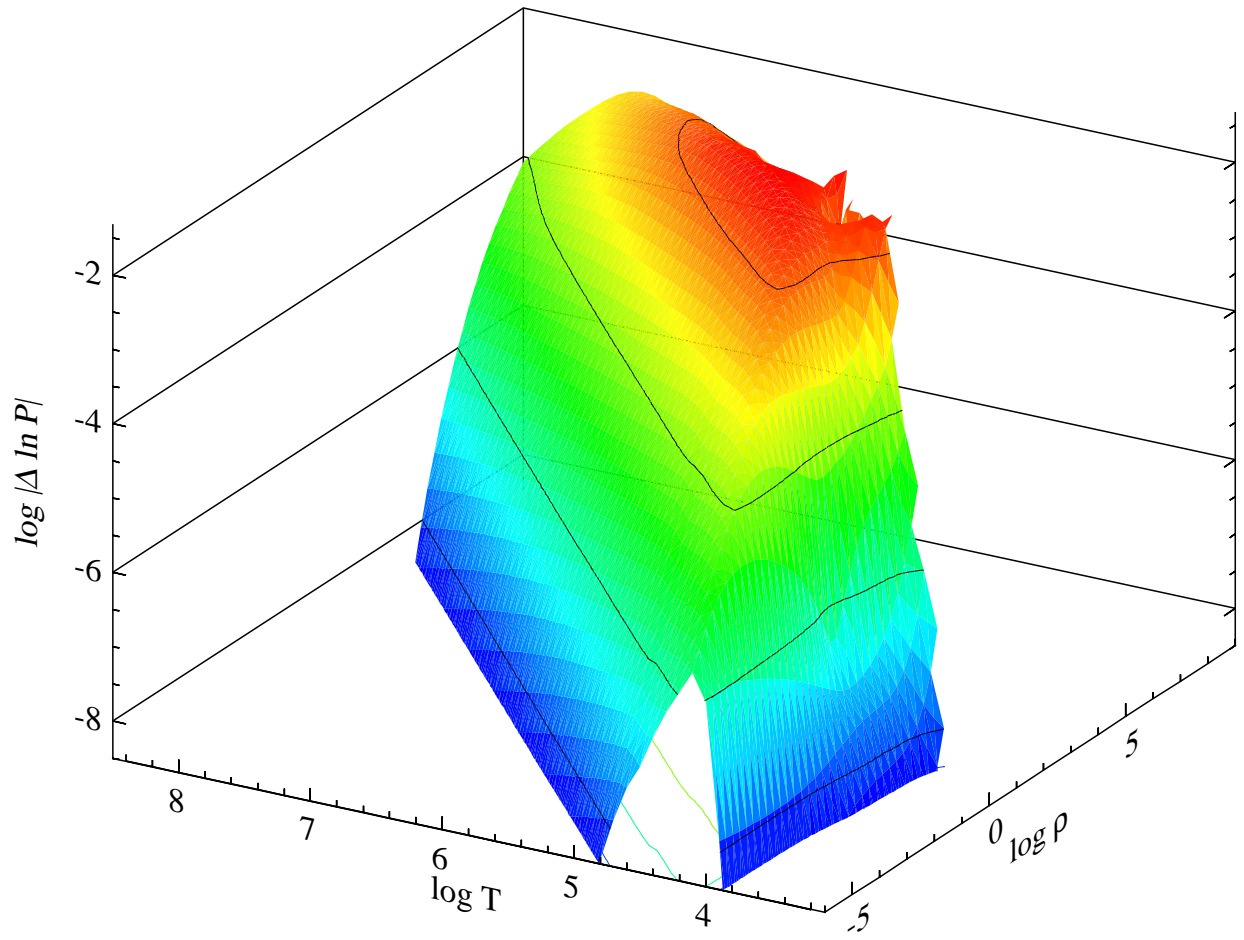
Fig. 7.— The same as figure 6 except all calculations were done for a 0.1- $M_\odot$  model.



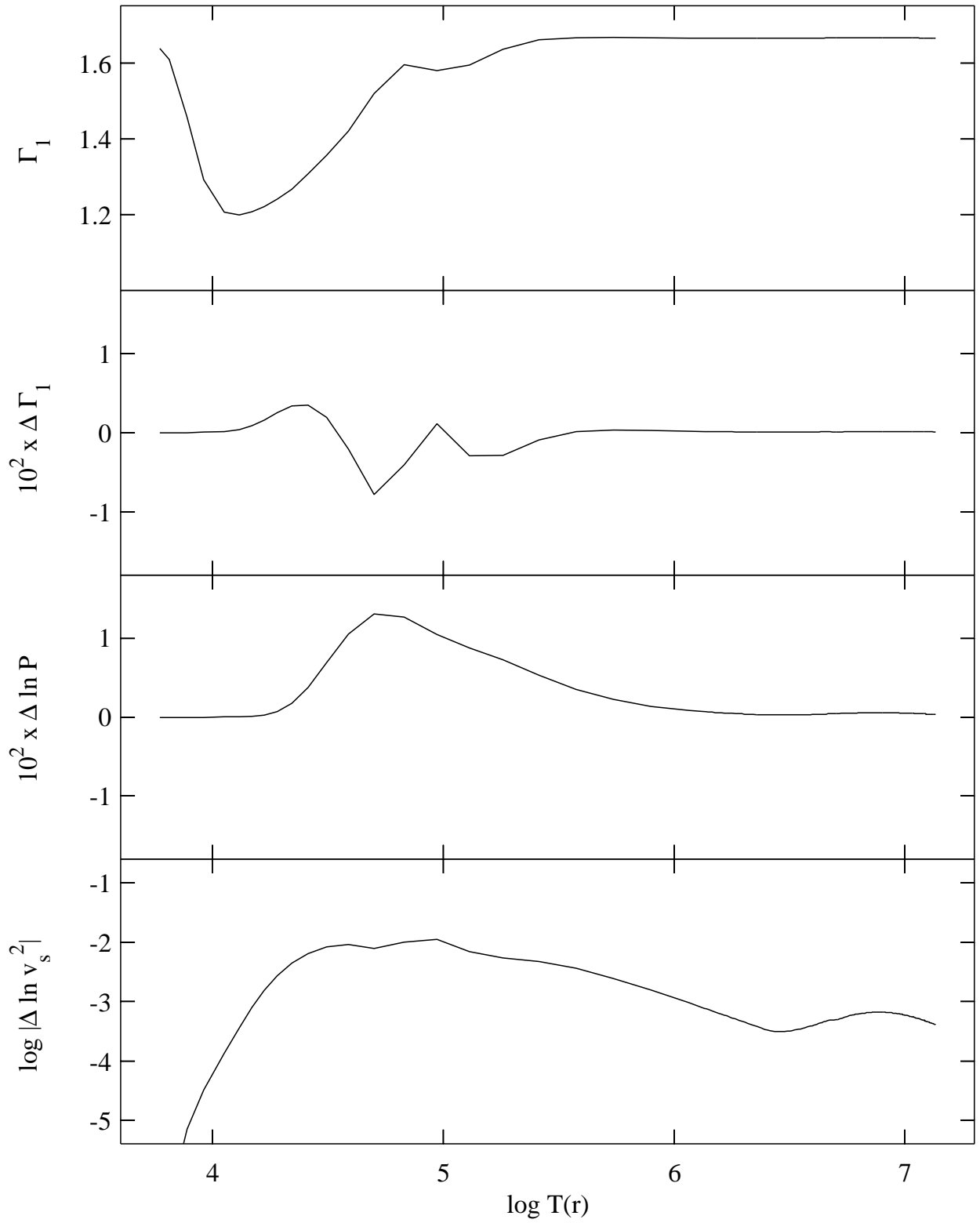








Results for a solar-mass model



Results for a 0.1-solar-mass model

